Structures of incommensurate and commensurate composite crystals Rb_xMnO_2 (x = 1.3711, 1.3636)

Jürgen Nuss,[a] Steffen Pfeiffer,[a] Sander van Smaalen[b] and Martin Jansen[a]*

[a]Max Planck Institute for Solid State Research, Heisenbergstrasse 1, D-70569 Stuttgart, Germany, and [b]Laboratory of Crystallography, University of Bayreuth, D-95440 Bayreuth, Germany

Correspondence e-mail: j.nuss@fkf.mpg.de

$Rb_{1.3711}MnO_2$ ($Rb_{11}Mn_8O_{16}$) has been synthesized *via* the azide/nitrate route from a stoichiometric mixture of the precursors Mn_2O_3, $RbNO_3$ and RbN_3. The structure of this extremely air- and moisture-sensitive compound can best be described in terms of an incommensurate composite structure, built up by a honeycomb-like framework of Rb ions, as one subsystem and by a second subsystem of chains, consisting of edge-sharing $MnO_{4/2}$ tetrahedra. These two composite substructures interpenetrate in such a way that the manganate chain polyanions centre the channels of the Rb-honeycomb framework. Crystals transform by an aging process into $Rb_{1.3636}MnO_2$ ($Rb_{15}Mn_{11}O_{22}$), which has a similar structure but a different commensurate modulation. Two reasons can be established for the origin of the modulations: the charge ordering of Mn^{2+}/Mn^{3+} on one hand, and the incompatibility of the Mn—Mn and Rb—Rb separations on the other.

1. Introduction

Charge, spin and orbital ordering in extended solids showing low-dimensional substructures are regarded as crucial prerequisites for the occurrence of collective physical phenomena like high T_c superconductivity or pronounced magnetoresistance (Cava, 2005; Pratt *et al.*, 1991). In most instances the required mixed-valence state of the respective transition metal has been introduced by extrinsic doping. Such an approach, however, has the unfavourable side effect of broken translational symmetry (perturbed periodicity; Saitoh *et al.*, 2001; Chuang *et al.*, 2001).

Recently, we have developed the azide/nitrate route for the synthesis of alkali oxometallates that allows for a remarkably minute control and adjustment of the compositions, including the oxygen contents, of the targeted transition metallates, opening a versatile access to intrinsically doped extended oxides (Trinschek & Jansen, 1999*a,b*). Along this procedure periodic sodium oxocuprates (II/III) like $Na_3Cu_2O_4$ and $Na_8Cu_5O_{10}$ have been prepared (Sofin *et al.*, 2005), which are the first unambiguous manifestations of a Wigner crystal (Horsch *et al.*, 2005). Their structures are commensurably modulated along one direction (van Smaalen *et al.*, 2007).

Next to cuprates, mixed-valent manganates (III/IV) continue to be in focus, because of the strong magnetoresistance they show (Coey *et al.*, 1999). Employing the azide/nitrate route, a new family of +2/+3 mixed-valent virtually one-dimensional oxomanganates $K_{29}Mn_{17}O_{34}$, $Rb_{11}Mn_8O_{16}$ and $Cs_4Mn_3O_6$ has been discovered (Pfeiffer *et al.*, 2010). In a first attempt their crystal structures were solved and refined assuming large supercells. However, some inconsistencies in the geometric structural features as well as in the displacement parameters indicate that this former treatment was not fully

Table 1
Experimental details.

For all structures: $Z = 16$. Experiments were carried out with Mo $K\alpha$ radiation using a CCD, APEX I diffractometer. Absorption was corrected for by multi-scan methods, semi-empirical (using intensity measurements) absorption correction with *SADABS* (Sheldrick, 2008a). Refinement was with 0 restraints. For wave vectors

$$W^1 = \begin{pmatrix} 1 & 0 & 0 & 0 \\ 0 & 1 & 0 & 0 \\ 0 & 0 & 1 & 0 \\ 0 & 0 & 0 & 1 \end{pmatrix}; \ W^2 = \begin{pmatrix} 1 & 0 & 0 & 0 \\ 0 & 1 & 0 & 0 \\ 0 & 0 & 0 & 1 \\ 0 & 0 & 1 & 0 \end{pmatrix}.$$

	$Rb_{11}Mn_8O_{16}$	$Rb_{15}Mn_{11}O_{22}$
Crystal data		
Chemical formula	$Mn_{0.729}O_{1.458}Rb$	$Mn_{0.733}O_{1.467}Rb$
M_r	148.8	149.2
Crystal system, space group	Orthorhombic, $Fddd(00\gamma)ss0$†	Orthorhombic, $Fddd(00\gamma)ss0$†
Wave vectors	$\mathbf{q} = 1.45870\mathbf{c}$	$\mathbf{q} = 1.46667\mathbf{c}$
Subsystem 1	Rb	Rb
a_1, b_1, c_1 (Å)	12.2070 (8), 20.1548 (14), 3.9753 (3)	12.1639 (4), 20.1013 (7), 3.9865 (2)
V_1 (Å³)	978.04 (12)	974.74 (7)
Modulation wavevector $\mathbf{q}_1$	0 0 0.68553 (3) $\simeq$ 11/16	0 0 15/22 $\simeq$ 0.68182
Z (subsystem 1)	16	16
Subsystem 2	MnO_2	MnO_2
a_2, b_2, c_2 (Å)	12.2070 (8), 20.1548 (14), 2.7252 (2)	12.1639 (4), 20.1013 (7), 2.7181 (2)
V_2 (Å³)	671.6 (1)	664.6 (1)
Modulation wavevector $\mathbf{q}_2$	0 0 1.45873 (3) $\simeq$ 16/11	0 0 22/15 (1.46667)
Z (subsystem 2)	8	8
Supercell a, b, c (Å)	12.2070 (8), 20.1548 (14), 43.666 (2)	12.1639 (4), 20.1013 (7), 59.798 (2)
t_0	1/44	1/20
Supercell space group	$F222$ (No. 22)	$Fddd$ (No. 70)
Z (supercell)	16×8	16×11
μ (mm⁻¹)	23.39	23.57
ρ_{calc} (Mg m⁻³)	4.038	4.066
Crystal form, colour	Rod, black	Rod, black
Crystal size (mm)	$0.30 \times 0.15 \times 0.10$	$0.30 \times 0.15 \times 0.10$
Data collection		
T_{min}, T_{max}	0.055, 0.156	0.059, 0.166
No. of measured, independent and observed [$I > 2\sigma(I)$] reflections	57 761, 11 525, 4058	79 001, 9909, 2130
R_{int}	0.059	0.096
Refinement		
$R[F^2 > 2\sigma(F^2)]$, $wR(F^2)$, S	0.041, 0.050, 1.18	0.041, 0.059, 1.17
No. of reflections	11 525	9909
No. of parameters	139	143
$\Delta\rho_{max}, \Delta\rho_{min}$ (e Å⁻³)	1.67, −2.04	5.04, −3.19

Computer programs used: *SMART* (Bruker AXS, 1997), *SAINT* (Bruker AXS, 2008), *SADABS* (Sheldrick, 2008a), *JANA*2006 (Petricek *et al.*, 2006), *SHELXTL* (Sheldrick, 2008b), *ATOMS* (Dowty, 2008). † Symmetry operations: (1) x_1, x_2, x_3, x_4; (2) $-x_1, -x_2 + \frac{1}{2}, x_3 + \frac{1}{2}, x_4$; (3) $-x_1 + \frac{1}{2}, x_2, -x_3 + \frac{1}{2}, -x_4 + \frac{1}{2}$; (4) $x_1, -x_2 + \frac{1}{2}, -x_3 + \frac{1}{2}, -x_4 + \frac{1}{2}$; (5) $-x_1 + \frac{1}{4}, -x_2 + \frac{1}{4}, -x_3 + \frac{1}{4}, -x_4$; (6) $x_1 + \frac{3}{4}, x_2 + \frac{1}{4}, -x_3 + \frac{3}{4}, -x_4$; (7) $x_1 + \frac{1}{4}, -x_2 + \frac{1}{4}, x_3 + \frac{1}{4}, x_4 + \frac{1}{2}$; (8) $-x_1 + \frac{1}{4}, x_2 + \frac{1}{4}, x_3 + \frac{1}{4}, x_4 + \frac{1}{2}$; (9) $x_1, x_2 + \frac{1}{2}, x_3 + \frac{1}{2}, x_4$; (10) $-x_1, -x_2, x_3, x_4$; (11) $-x_1 + \frac{1}{2}, x_2 + \frac{1}{2}, -x_3, -x_4 + \frac{1}{2}$; (12) $x_1, -x_2, -x_3, -x_4 + \frac{1}{2}$; (13) $-x_1 + \frac{1}{4}, -x_2 + \frac{3}{4}, -x_3, -x_4$; (14) $x_1 + \frac{3}{4}, x_2 + \frac{3}{4}, -x_3 + \frac{1}{4}, -x_4$; (15) $x_1 + \frac{1}{4}, -x_2 + \frac{3}{4}, x_3 + \frac{3}{4}, x_4 + \frac{1}{2}$; (16) $-x_1 + \frac{1}{4}, x_2 + \frac{3}{4}, x_3 + \frac{3}{4}, x_4 + \frac{1}{2}$; (17) $x_1 + \frac{1}{2}, x_2, x_3 + \frac{1}{2}, x_4$; (18) $-x_1 + \frac{1}{2}, -x_2 + \frac{1}{2}, x_3, x_4$; (19) $-x_1, x_2, -x_3, -x_4 + \frac{1}{2}$; (20) $x_1 + \frac{1}{2}, -x_2 + \frac{1}{2}, -x_3, -x_4 + \frac{1}{2}$; (21) $-x_1 + \frac{3}{4}, -x_2 + \frac{1}{4}, -x_3 + \frac{3}{4}, -x_4$; (22) $x_1 + \frac{1}{4}, x_2 + \frac{1}{4}, -x_3 + \frac{1}{4}, -x_4$; (23) $x_1 + \frac{3}{4}, -x_2 + \frac{1}{4}, x_3 + \frac{3}{4}, x_4 + \frac{1}{2}$; (24) $-x_1 + \frac{3}{4}, x_2 + \frac{1}{4}, x_3 + \frac{3}{4}, x_4 + \frac{1}{2}$; (25) $x_1 + \frac{1}{2}, x_2 + \frac{1}{2}, x_3, x_4$; (26) $-x_1 + \frac{1}{2}, -x_2, x_3 + \frac{1}{2}, x_4$; (27) $-x_1, x_2 + \frac{1}{2}, -x_3 + \frac{1}{2}, -x_4 + \frac{1}{2}$; (28) $x_1 + \frac{1}{2}, -x_2, -x_3 + \frac{1}{2}, -x_4 + \frac{1}{2}$; (29) $-x_1 + \frac{3}{4}, -x_2 + \frac{3}{4}, -x_3 + \frac{1}{4}, -x_4$; (30) $x_1 + \frac{1}{4}, x_2 + \frac{3}{4}, -x_3 + \frac{3}{4}, -x_4$; (31) $x_1 + \frac{3}{4}, -x_2 + \frac{3}{4}, x_3 + \frac{1}{4}, x_4 + \frac{1}{2}$; (32) $-x_1 + \frac{3}{4}, x_2 + \frac{3}{4}, x_3 + \frac{1}{4}, x_4 + \frac{1}{2}$.

adequate. Here we report on a more accurate crystallographic analysis of Rb_xMnO_2 by using the superspace approach (van Smaalen, 2004).

2. Experimental

2.1. Synthesis

The starting materials for the preparation of the title compounds were Mn_2O_3 (99.9% Chempur, Karlsruhe, Germany) and $RbNO_3$ (99%, Johnson Matthey, Sulzbach, Germany). The respective azide was synthesized from aqueous HN_3 and rubidium carbonate (99% Johnson Matthey; Brauer, 1975). The starting materials were mixed in the ratio required according to the following.

$$29RbN_3 + 4RbNO_3 + 12Mn_2O_3 \rightarrow 3Rb_{11}Mn_8O_{16} + 45.5N_2 \tag{1}$$
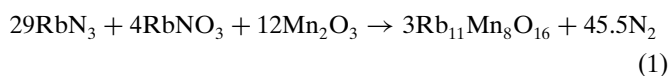
The mixtures were ground thoroughly in an agate mortar and pressed in pellets under 10^5 N, dried under vacuum (10^{-3} mbar) at 400 K for 12 h, and placed under argon in a
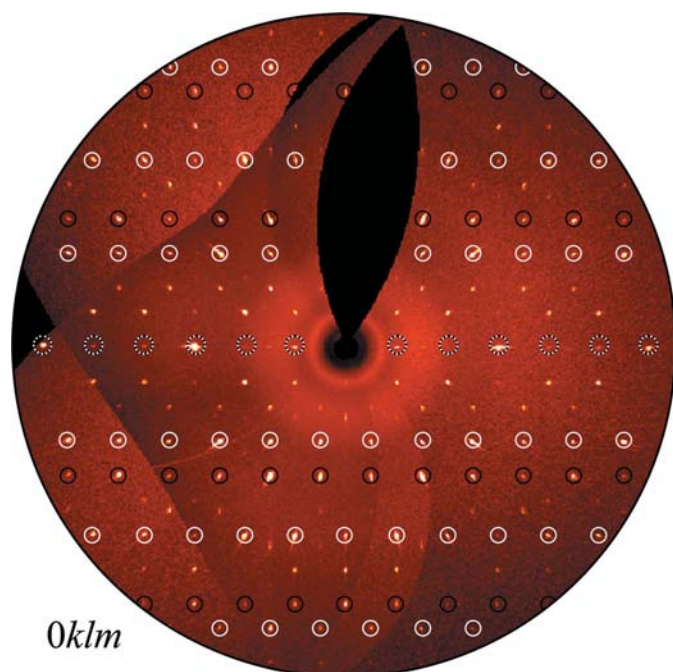
Figure 1
Reciprocal layer 0klm of the $Rb_{11}Mn_8O_{16}$ single crystal. The main reflections of the Rb subsystem (0kl0) are emphasized by black circles, and those of the [MnO_2] subsystem (0k0m) by white circles. The unmarked reflections between are satellites 0klm.

Table 2
Reliability factors (%) of various reflection groups for the best refinements.

	N_{ref}(all)	N_{ref}(obs)	R_F(obs)	R_F(all)	wR_{F^2}(all)
$Rb_{11}Mn_8O_{16}$					
All	11 525	4038	4.11	16.07	5.03
Main	1662	1195	2.74	4.13	3.95
$m = 1$	2599	1685	3.78	8.02	3.87
$m = 2$	1972	794	8.05	23.72	7.01
$m = 3$	1876	322	19.5	64.1	20.2
$m = 4$	1888	46	59.9	134.1	63.2
$m = 5$	1528	16	48.2	189.2	67.8
$Rb_{15}Mn_{11}O_{22}$					
All	9909	2130	4.12	27.87	5.87
Main	1052	729	3.08	4.84	3.57
$m = 1$	1665	908	4.40	11.60	5.12
$m = 2$	1267	381	7.49	30.45	9.51
$m = 3$	1178	101	16.3	85.9	28.1
$m = 4$	1200	7	24.4	141.2	53.5
$m = 5$	1212	3	25.4	219.5	62.7

closed steel container, provided with a silver inlay, that allows the N_2 overpressure to release (Trinschek & Jansen, 1999a,b). In a flow of dried argon the following temperature profile was applied: $298 \rightarrow 533$ K (100 K h^{-1}); $533 \rightarrow 653$ K (5 K h^{-1}); $653 \rightarrow 773$ K (20 K h^{-1}) and subsequent annealing for 30 h at 773 K.

The black powders obtained were very sensitive to humid air and were therefore sealed in glass ampoules under argon atmosphere and all the remaining procedures using these substances were performed in an inert atmosphere of purified argon.

Single crystals of $Rb_{11}Mn_8O_{16}$ have been grown by annealing of the starting materials (RbN_3, $RbNO_3$, Mn_2O_3) at 723 K; however, applying excess rubidium (Rb:Mn = 2:1) provided better crystal growth. Afterwards the primary product was pressed in a pellet, placed in a silver crucible, which was sealed in a glass ampoule under dried argon, and annealed for an additional 500 h at 723 K.

2.2. X-ray diffraction

For X-ray diffraction experiments, single crystals were selected in a dry-box (M. Braun, Garching, Germany) under an argon atmosphere (< 0.1 p.p.m. O_2, H_2O) and mounted in sealed glass capillaries. Collection of the diffraction intensities was performed on a SMART APEX I three-circle diffractometer with an APEX I CCD detector (Bruker AXS, 1997) at 296 K. The intensities were integrated using the *SAINT* program (Bruker AXS, 2008). An absorption correction was applied using *SADABS* (Sheldrick, 2008a). Experimental details are given in Table 1.[1]

3. Structure determination

The diffraction intensities of the first set of crystals, measured directly after synthesis, were indexed and integrated on the basis of the orthorhombic crystal system, with $a = 12.207$, $b = 20.155$ and $c = 43.666$ Å. From the systematic extinctions the F-centred orthorhombic Bravais type was deduced, and $F222$ proved to be an appropriate space group during the structure determination and refinement. However, on re-investigating the crystals 6 months later it became obvious that the translation symmetry had changed through aging. The aged crystals were still orthorhombic, but with $a = 12.164$, $b = 20.101$ and $c = 59.798$ Å. The systematic extinctions observed (hkl: all odd or all even, 0kl: $k + l = 4n$, h0l: $h + l = 4n$, and hk0: $h + k = 4n$) led to the space group $Fddd$, unambiguously.

The structure solutions and refinements of both data sets, performed using *SHELXTL* (Sheldrick, 2008b), resulted in the compositions $Rb_{11}Mn_8O_{16}$ ($Rb_{1.375}MnO_2$) and $Rb_{15}Mn_{11}O_{22}$ ($Rb_{1.364}MnO_2$). However, for some of the Rb ions and most of the O atoms, unusually large displacement parameters resulted during the structure refinement. Using split models did not provide more satisfying results. Noteworthy is the structure refinement of $Rb_{15}Mn_{11}O_{22}$ which appeared to be much more accurate than that of $Rb_{11}Mn_8O_{16}$, as reflected by better R values and more reasonable displacement parameters (Pfeiffer *et al.*, 2009, 2010).

Despite the significant uncertainties in the structure refinements, the characteristic building principle of both structures, one-dimensional polyanions $^1_\infty[MnO_2]^{n-}$ embedded in channels formed by Rb ions have been revealed, unambiguously.

---

[1] Supplementary data for this paper are available from the IUCr electronic archives (Reference: CK5041). Services for accessing these data are described at the back of the journal.

According to careful inspection of the reciprocal space using the *Precession* module of the Bruker Suite software package (Bruker AXS, 2008) – which allows for a detailed exploration of the reciprocal space without being restricted to integer *hkl* values (Nuss *et al.*, 2007) – most of the nominally allowed higher-order satellite reflections were missing (Fig. 1 and Table 2). This feature, taken together with the deficiencies in our preliminary structure models, are characteristic warning signs either for twinned (Herbst-Irmer & Sheldrick, 1998) or modulated crystals (van Smaalen *et al.*, 2007).

Indeed the diffraction intensities can be indexed by assuming commensurate composite structures consisting of two subcells with different *c* axes: $c_1 = 43.666/11 = 3.970$ Å and $c_2 = 43.666/16 = 2.729$ Å for $Rb_{11}Mn_8O_{16}$ and $c_1 = 59.798/15 = 3.986$ Å and $c_2 = 59.798/22 = 2.718$ Å for $Rb_{15}Mn_{11}O_{22}$. All observed reflections can be indexed with four integer indices (*hklm*) with respect to the reciprocal lattice of the Rb subsystems applying modulation wavevectors of $\mathbf{q}_1 = 16/11\mathbf{c}_1^*$ and $\mathbf{q}_1 = 22/15\mathbf{c}_1^*$. Fig. 1 shows the reciprocal layer 0*klm* for $Rb_{11}Mn_8O_{16}$ with the main reflections (0*kl*0, 0*k*0*m*) marked for both subcells; all visible intensities can be indexed including the satellites 0*klm*.

To obtain *hklm* datasets, the three-dimensional data were re-indexed with respect to $\mathbf{a}_1^*$, $\mathbf{b}_1^*$, $\mathbf{c}_1^*$ and $\mathbf{q}_1$. Calculations were performed using *JANA*2006 (Petricek *et al.*, 2006). The symmetry, for both crystals, can be described by the ortho-rhombic superspace group $Fddd(00\gamma)ss0$, which was derived on the basis of the reflection conditions observed (Janssen *et*
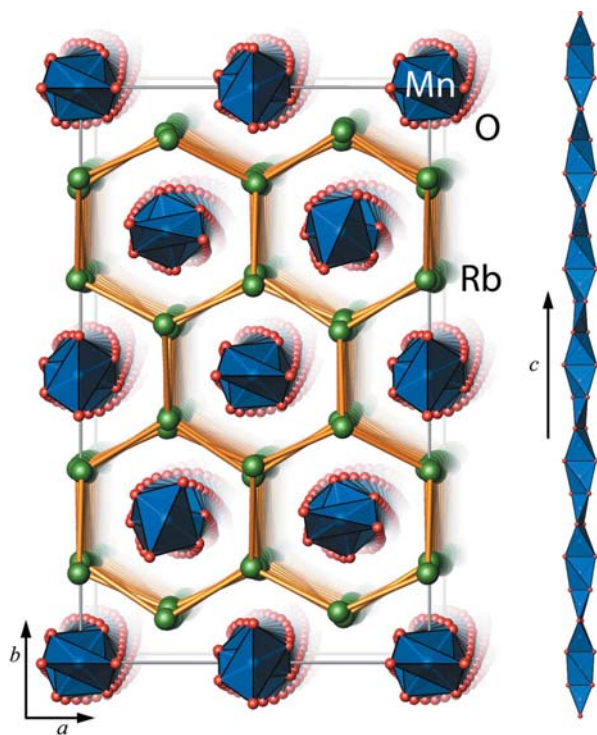
al., 1995). The three-dimensional space groups *F*222 and *Fddd* of the supercells can be recovered by selecting the sections of superspace defined by $t_0 = 1/44$ for $Rb_{11}Mn_8O_{16}$ and $t_0 = 1/20$ for $Rb_{15}Mn_{11}O_{22}$.

The starting model for the basis structure was derived from the superstructure in three-dimensional space with Rb at (0, 0.333, 0), Mn at (0, 0, $\frac{1}{4}$) and O at (0.080, 0.048, $\frac{3}{4}$). A crenel function (Evain & Petricek, 2004) has been used to model the occupancy of the O atom to construct the necessary fourfold coordination of manganese (alternatively a saw-tooth function can be used and leads to an equivalent starting model). Superspace models for the crystal structures were developed by refinement of the basic structures against the main reflections ($Rb_{11}Mn_8O_{16}$: $R_{obs} = 0.2816$, $Rb_{15}Mn_{11}O_{22}$: $R_{obs} = 0.3163$) and by subsequent introduction of modulation parameters and refinements against the complete datasets including satellite reflections. It was necessary to introduce up to sixth-order harmonic coefficients of the modulation functions for Rb and Mn, and up to fourth-order harmonic coef-
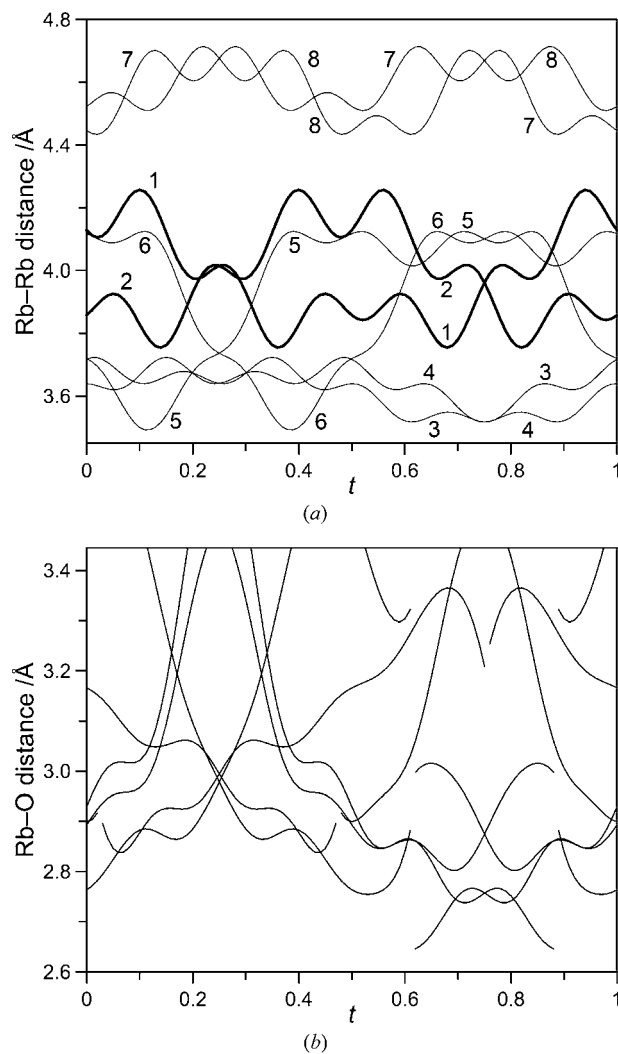
Figure 2
Left: perspective representation of the crystal structure of $Rb_{15}Mn_{11}O_{22}$, with margins of the unit cell (grey); the shortest Rb—Rb contacts are drawn by orange sticks. Right: MnO_2 chain of edge-sharing MnO_4 tetrahedra in the **c** direction.

Figure 3
Coordination of Rb in $Rb_{11}Mn_8O_{16}$. (*a*) *t*-plot of the eight Rb—Rb (1–8) distances; the two Rb—Rb distances (1–2, bold lines) are oriented along the *c* direction, they vary between 3.7 and 4.3 Å. (*b*) *t*-plot of the Rb—O distances.

ficients for O. The introduction of sixth-(third)-order harmonic coefficients for the modulation of the anisotropic displacement parameters (ADPs) for Rb (Mn, O) results in better fits.

Refinement with an incommensurate modulation led to significantly lower R values (R_{obs} = 0.0411) than the commensurate approach (R_{obs} = 0.0456) for $Rb_{11}Mn_8O_{16}$. In the case of $Rb_{15}Mn_{11}O_{22}$, incommensurate modulation functions do not improve the R values (R_{obs} = 0.0399 rather than 0.0412). The incommensurability of $Rb_{11}Mn_8O_{16}$ implies that the supercell of c = 43.666 Å can only be an approximation. Therefore, the lattice parameters of the two subsystems have

been independently refined against the diffraction data. It turns out that the lattice parameter of the Rb subsystem is slightly larger than 43.666/11 with $c1$ = 3.9753 (3) Å, and that the lattice parameter of the MnO_2 subsystem is slightly smaller than 43.666/16 with c_2 = 2.7252 (2) Å. The composition then is $Rb_{1.3711}MnO_2$ or $Rb_{10.97}Mn_8O_{16}$.

The corresponding R values can also be obtained by refinements in the supercells, but the number of parameters in the superspace approach is smaller than that in the supercell structure: 139 versus 329 for $Rb_{11}Mn_8O_{16}$ (Pfeiffer et al., 2010) and 143 versus 224 for $Rb_{15}Mn_{11}O_{22}$ (Pfeiffer et al., 2009). Only three crystallographically independent atomic sites are necessary for the incommensurate structure model instead of 46 ($Rb_{11}Mn_8O_{16}$) and 31 ($Rb_{15}Mn_{11}O_{22}$) for the supercell models. Finally, there are obvious inconsistencies in the displacement parameters of Rb and O atoms, which are in some cases much too large for the supercell approach (Pfeiffer
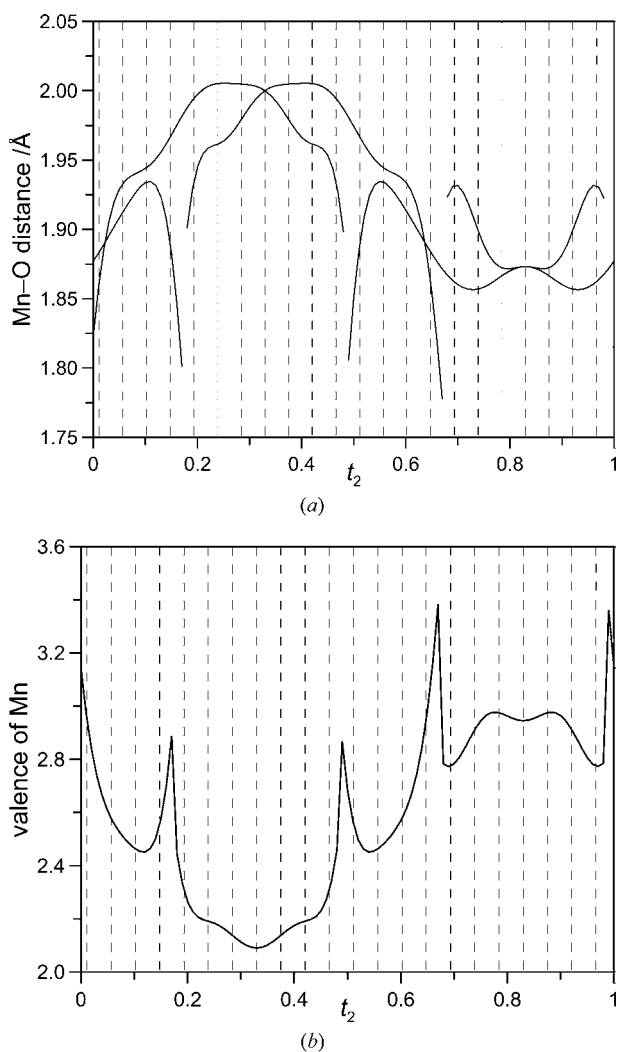
Figure 4
Coordination of Mn in $Rb_{15}Mn_{11}O_{22}$. (a) t-plot of the four Mn—O distances of the first coordination shell; vertical dashed lines indicate those values of t_2 that are realised in the commensurate composite structure. (b) t-plot of the valence of Mn obtained by the bond-valence method. The t-parameter in the second subsystem is $t_2 = t/0.682 = t/(15/22)$. Bond-valence parameters due to Brese & O'Keeffe (1991) have been used, with b = 0.37 Å and R_0(Rb—Rb) = 3.68 Å; R_0(Rb—O) = 2.11 Å; R_0(Rb—Mn) = 2.95 Å; R_0(Mn—Mn) = 2.34 Å; R_0(Mn^{III}—O) = 1.76 Å; R_0(Mn^{II}—O) = 1.79 Å; R_0(O—O) = 1.48 Å. The sharp features [very short bonds (a), pronounced maxima (b)] are artefacts owing to the special form of the modulation functions of oxygen; they are not realised in the commensurate composite structure.
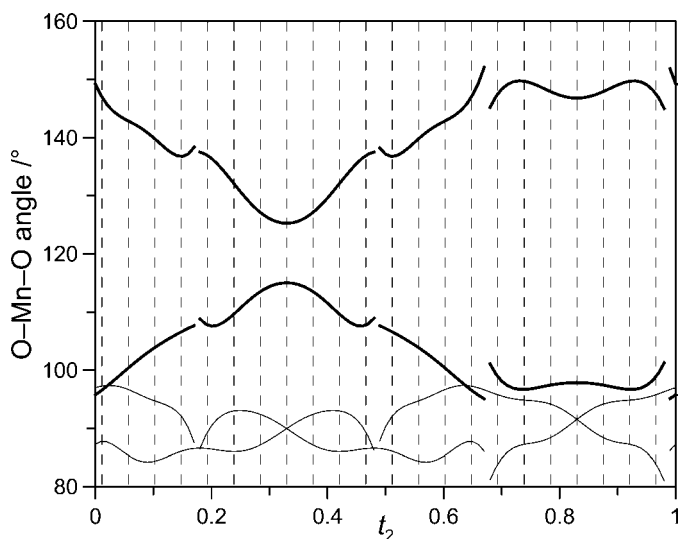
Figure 5
Coordination of Mn in $Rb_{15}Mn_{11}O_{22}$: the six O—Mn—O angles as a function of the parameter t_2 (vertical dashed lines indicate those values of t_2 that are realised in the commensurate composite structure. Bold lines have to be counted twice due to symmetry relations).
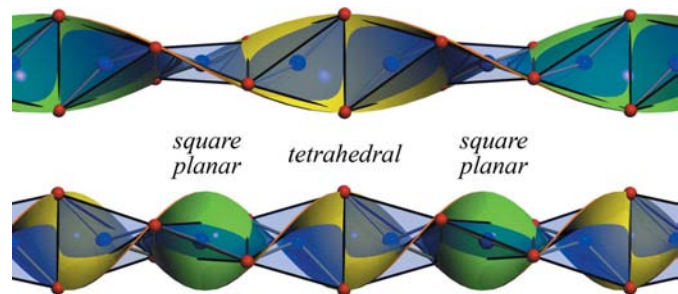
Figure 6
Fragment of the crystal structure of $Rb_{15}Mn_{11}O_{22}$ with a right-handed (top) and left-handed (below) helicoidal surface, emphasizing the helicoidally shaped MnO_2 chain with alternation of distorted tetrahedral and square-planar coordination of manganese (same colour code as Fig. 2).

et al., 2009, 2010). Both types of atoms (Rb, O) are much more affected by modulations than the Mn atoms.

Table 1 lists the final results, including lattice parameters of the subcells and supercells; itemized R values are listed in Table 2. Atomic coordinates and isotropic displacement parameters, and additional parameters for the superspace model are available in the supplementary material.

4. Discussion

The two new mixed-valence oxomanganates $Rb_{11}Mn_8O_{16}$ and $Rb_{15}Mn_{11}O_{22}$ crystallize as composite crystals in the same $(3 + 1)$-dimensional superspace group $Fddd(00\gamma)ss0$ with slightly different periodicities of the Rb subsystems and of the MnO_2 subsystems along the chain directions **c**. Figs. 2–7 provide different views of the crystal structure and t-plots of interatomic distances, angles and valence values.

The first subsystem of Rb_xMnO_2 is a channel structure formed by Rb ions whose projection along the c axis can be regarded as a honeycomb-like framework (Fig. 2). The most prominent structural feature is the second subsystem, which is based on edge-sharing $MnO_{4/2}$ tetrahedra, forming infinite chains along **c** (Fig. 2). These one-dimensional polyanions $\frac{1}{\infty}[MnO_2]^{n-}$ fill the channels of the Rb subsystem.

Bonding between the mutually incommensurate subsystems is governed by the Rb and O atoms. The incommensurability implies an infinite number of different coordinations of Rb by O with a shortest Rb—O distance of 2.5 Å in the non-modulated structure. Modulations of Rb of up to 0.3 Å and of oxygen of up ~ 1.0 Å have the effect of increasing the shortest distance towards the more reasonable value of 2.65 Å, and of reducing the variation of the shortest Rb—O bond between different coordination polyhedra (Fig. 3). The modulation of Rb is restricted by the condition that Rb—Rb contacts which are too short cannot be present, as is indeed fulfilled by the

modulated structure (minimum Rb—Rb distance is 3.5 Å). The average Rb—Rb distance corresponds to the length of the c_1 axis. This ideal Rb—Rb contact also determines the composition of the Rb_xMnO_2 ($x \simeq 1.37$) compounds, as can be clearly seen in comparison to similar potassium and caesium compounds. Potassium ions are smaller than rubidium ions resulting in a composition of K_xMnO_2 with larger $x = 1.706$, while Cs is larger than Rb resulting in a composition with smaller Cs contents, $Cs_{1.333}MnO_2$. The required charge neutrality is provided by the balance between Mn^{2+} and Mn^{3+}, which thus is different in these three compounds (Pfeiffer *et al.*, 2010).

The modulation of oxygen is restricted by the requirements of optimal coordinations of manganese and of rubidium. The largest amplitude is in the **ab** plane and it is responsible for the screw-like character of the MnO_2 chains. At the same time, these shifts describe displacements of oxygen tangential to the chains of Rb ions and thus have a relatively small influence on the Rb—O distances. Mn atoms are not involved in intersubsystem bonding. Concomitantly, their modulation is the smallest of the three crystallographically independent atoms, with an amplitude of 0.08 Å.

The Mn—O bond does not have one optimal value, but variations of the coordination of Mn reflect the two valence states of this atom, with on average longer Mn—O bonds for Mn^{2+} than for Mn^{3+}. The four Mn—O bonds are pairwise equal (Fig. 4a). The relatively large variation between 1.80 and 2.05 Å can indeed be explained by the two valence states of Mn as shown by the valences computed by the bond-valence method (Fig. 4b; Brown, 2002; Brese & O'Keeffe, 1991).

The helical MnO_2 chains are composed of strongly distorted $MnO_{4/2}$ tetrahedra. Two of the six O—Mn—O angles are ~ 90° (thin lines in Fig. 5), and they show smaller variations compared with the other four angles. The latter reflect the type of screwing of the O atoms. Starting from approximately 120°, the angles split into pairs of 150 and 100° (bold lines in Fig. 5). The coordination of manganese can be described as varying between distorted tetrahedral and distorted square planar coordinations (Fig. 6). The comparison of Figs. 4(b) and 5 shows that Mn^{2+} is in a distorted tetrahedral coordination and Mn^{3+} approaches a square-planar-like coordination. Although many coordinations indicate an intermediate valence state of Mn, an approximate value of 1:2 can be derived for the tetrahedral:planar and the Mn^{2+}:Mn^{3+} ratios (vertical dashed lines in Figs. 4b and 5). This ratio is in accordance with the mixed-valence character of manganese as can be determined from the compositions of the compounds Rb_xMnO_2 ($x = 1.371$ and 1.364), with Mn^{2+}:Mn^{3+} = $(x - 1)$: $(2 - x)$, *i.e.* 1: 2 for $x = 1.333$. The valence state of manganese is furthermore reflected in the Mn—Mn distances along the chains, which are on average shorter for Mn^{2+} than for Mn^{3+} (Fig. 7), in accordance with higher repulsive forces between the latter ions. Finally, the distorted tetrahedral coordination of Mn^{2+} with $[Ar]3d^5$ electron configuration as opposed to the distorted square-planar coordination of Mn^{3+} ($[Ar]3d^4$) is in accordance with the preference of a d^4 low-spin configuration for the latter coordination.
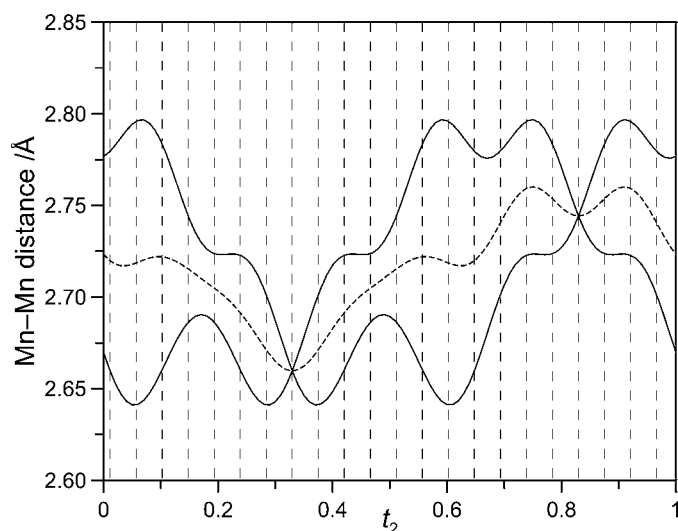

Figure 7
Coordination of Mn in $Rb_{15}Mn_{11}O_{22}$: t-plot of the two shortest Mn—Mn distances (solid lines), and their average (dashed line) along the chains.

Several reasons can be considered for the structural transition of $Rb_{11}Mn_8O_{16}$ into $Rb_{15}Mn_{11}O_{22}$ by aging.

(i) $Rb_{15}Mn_{11}O_{22}$ is the more stable compound at room temperature, while $Rb_{11}Mn_8O_{16}$ is more stable at the higher temperature used for synthesis.

(ii) $Rb_{11}Mn_8O_{16}$ is only formed because of the excess rubidium during synthesis, while this compound kept at ambient conditions spontaneously loses some rubidium.

(iii) The loss of rubidium is induced by oxidation or hydrolysis, thus being responsible for the change of composition from $Rb_{1.3711}MnO_2$ to $Rb_{1.3636}MnO_2$.

5. Conclusions

Two reasons have been established for the origin of the modulations: charge ordering of Mn^{2+}/Mn^{3+} and the composite character of the two compounds, which requires the resolution of inter-subsystem contacts. Together they have resulted in displacive modulations, mainly of Rb and O atoms.

The structures of incommensurate and commensurate Rb_xMnO_2 compounds ($x = 1.3711$ and $x = 15/11 = 1.3636$) share many features, with remarkably similar coordinations of the Mn atoms. This supports the idea that different compounds, with common structural features, can be described by a similar basic structure and similar modulation functions within the unified superspace approach (Perez-Mato *et al.*, 1999), although modulation functions of the different compounds can differ in detail (Guevarra *et al.*, 2007).

The rubidium oxomanganates show structural features, which are also similar to the recently discovered family of mixed-valence sodium oxocuprates (II/III), where charge ordering of square-planar coordinated Cu^{2+} and Cu^{3+} ions are also the origin of modulations (Horsch *et al.*, 2005; van Smaalen *et al.*, 2007). Finally, there are similarities to the family of chain-like composite crystals derived from the hexagonal perovskite-type structure, like $Sr_{14/11}CoO_3$ (Gourdon *et al.*, 1999) and $Sr_{1.2872}NiO_3$ (Evain *et al.*, 1998). These compounds also possess honeycomb-like frameworks of strontium atoms, but the channels are then filled with chains of face-sharing $CoO_{6/2}$ or $NiO_{6/2}$ polyhedra of alternating distorted octahedron and distorted trigonal prismatic geometries.

References

Brauer, G. (1975). *Handbuch der Präparativen Anorganischen Chemie*, Vol. 1, 3rd ed., pp. 458–459. Stuttgart: Enke Verlag.

Brese, N. E. & O'Keeffe, M. (1991). *Acta Cryst.* B**47**, 192–197.

Brown, I. D. (2002). *The Chemical Bond in Inorganic Chemistry; The Bond Valence Method.* Oxford University Press.

Bruker AXS (1997). Bruker Molecular Analysis Research Tool, Version 5.632. Bruker AXS Inc., Madison, Wisconsin, USA.

Bruker AXS (2008). *SAINT*, Version 7.60A. Bruker AXS Inc., Madison, Wisconsin, USA.

Cava, R. J. (2005). *Chem. Commun.* **43**, 5373–5377.

Chuang, Y. D., Gromoko, A. D., Dessau, D. S. Kimura, T. & Tokura, Y. (2001). *Science*, **292**, 1509–1513.

Coey, J. M. D., Viret, M. & Molnár, S. von (1999). *Adv. Phys.* **48**, 167–293.

Dowty, E. (2008). *ATOMS*, Version 6.3.4. Shape Software, Kingsport, Tennessee, USA.

Evain, M., Boucher, F. & Gourdon, O. (1998). *Chem. Mater.* **10**, 3068–3076.

Evain, M. & Petricek, V. (2004). *Ferroelectrics*, **305**, 43–48.

Gourdon, O., Petricek, V., Dusek, M., Bezdicka, P., Durovic, S., Gyepesova, D. & Evain, M. (1999). *Acta Cryst.* B**55**, 841–848.

Guevarra, J., Schönleber, A., van Smaalen, S. & Lichtenberg, F. (2007). *Acta Cryst.* B**63**, 183–189.

Herbst-Irmer, R. & Sheldrick, G. M. (1998). *Acta Cryst.* B**54**, 443–449.

Horsch, P., Sofin, M., Mayr, M. & Jansen, M. (2005). *Phys. Rev. Lett.* **94**, 076403.

Janssen, T., Janner, A., Looijenga-Vos, A. & de Wolff, P. M. (1995). *International Tables for Crystallography*, Vol. C, edited by A. J. C. Wilson, pp. 797–835. Dordrecht: Kluwer Academic Publishers.

Nuss, J., Ali, N. Z. & Jansen, M. (2007). *Acta Cryst.* B**63**, 719–725.

Perez-Mato, J. M., Zakhour-Nakhl, M., Weill, F. & Darriet, J. (1999). *J. Mater. Chem.* **9**, 2795–2808.

Petricek, V., Dusek, M. & Palatinus, L. (2006). *JANA2006*. Institute of Physics, Praha, Czech Republic.

Pfeiffer, S., Nuss, J. & Jansen, M. (2009). *Z. Kristallogr. New Cryst. Struct.* **224**, 377–378.

Pfeiffer, S., Nuss, J. & Jansen, M. (2010). *Z. Anorg. Allg. Chem.* **636**, 23–29.

Pratt, W. P., Lee, S. F., Slaughter, J. M., Loloee, R., Schroeder, P. A. & Bass, J. (1991). *Phys. Rev. Lett.* **66**, 3060–3063.

Saitoh, E., Okamoto, S., Takahashi, K. T., Tobe, K., Yamamoto, K., Kimura, T., Ishihara, S., Maekawa, S. & Tokura, Y. (2001). *Nature*, **410**, 180–183.

Sheldrick, G. M. (2008a). *SADABS*, Version 2008/1. University of Göttingen, Germany.

Sheldrick, G. M. (2008b). *Acta Cryst.* A**64**, 112–122.

Sofin, M., Peters, E.-M. & Jansen, M. (2005). *J. Solid State Chem.* **178**, 3708–3714.

Trinschek, D. & Jansen, M. (1999a). *Angew. Chem.* **111**, 234–235.

Trinschek, D. & Jansen, M. (1999b). *Angew. Chem. Int. Ed. Engl.* **38**, 133–135.

van Smaalen, S. (2004). *Z. Kristallogr.* **219**, 681–691.

van Smaalen, S., Dinnebier, R., Sofin, M. & Jansen, M. (2007). *Acta Cryst.* B**63**, 17–25.